Turkish Journal of Electrical Engineering & Computer Sciences

http://journals.tubitak.gov.tr/elektrik/

Research Article

Turk J Elec Eng & Comp Sci
(2016) 24: 3198 – 3211

doi:10.3906/elk-1406-177

Enhanced control of a DFIG-based system by sliding-mode control method during network disturbances

Saeed ABAZARI*, Sajad FARAJZADEH, Samad TAGHIPOUR BOROUJENI
Technical and Engineering Faculty, Shahrekord University, Shahrekord, Iran

Received: 24.06.2014 • **Accepted/Published Online:** 20.03.2015 • **Final Version:** 15.04.2016

Abstract: This paper presents a new method for control of the grid-side converter (GSC) of a doubly fed induction generator (DFIG) system under unbalanced and harmonic grid voltage conditions. The proposed controller is designed based on the sliding-mode control (SMC) method, and operates better than the current ones as the power quality of the DFIG is improved. The fluctuations in electromagnetic torque and stator reactive power are removed by control of the rotor-side converter (RSC). In addition, the GSC keeps the DC-link voltage at a reference value and mitigates not only fluctuations but also oscillations in steady injected active power to the network. Therefore, the output power of the system is free from any fluctuation and distortion. The control algorithm is implemented in the stationary reference frame and it is not necessary to extract voltage or current sequences in either of the converters. The proposed control algorithms are also robust against parameter variations and the resulting dynamic response is fast. The simulation results confirm the validity of the mentioned advantages and the effectiveness of the proposed method.

Key words: Doubly fed induction generator, unbalanced and harmonic voltage, rotor-side converter, grid-side converter, sliding-mode control

1. Introduction

A decreasing trend in fossil fuel sources and natural gases and the increase in energy prices have heightened the need for renewable energy technology. Among the different renewable energy types, wind energy is probably the most popular one. Due to the advantages of the doubly fed induction generator (DFIG), it is used extensively in wind power systems. Nonlinear and unbalanced loads as well as the grid faults cause some disturbances in the DFIG [1–3]. Unbalanced voltages at the DFIG terminals cause double line-frequency oscillations in the electromagnetic torque, and injected active and reactive powers to the grid [4]. The conventional control schemes of grid-connected DFIGs are generally based on a vector control algorithm with stator voltage orientation (SVO) [5,6] or stator flux orientation (SFO) [7,8]. In these methods, active and reactive powers are controlled through adjusting components of rotor current by proportional-integral (PI) controllers. The main drawback of these methods is that adjusting PI parameters is cumbersome. In addition, these controllers are sensitive to parameter variation, unbalanced condition, and harmonic disturbances.

In [9], a dual PI controller has been employed for adjusting both positive and negative components of the rotor current. In [10], an auxiliary PI controller has been added to the dual PI one, to adjust the rotor compensator current. A resonance PI controller is used to prevent positive and negative sequence extractions

*Correspondence: saeedabazari@yahoo.com

of rotor current [11–14]. Although the dynamic response is improved in [11–13], it is necessary to transfer the variables to the synchronous reference frame. As well as the complex procedure in [11–14], the methods are not robust enough against the parameter variations. In [15], a series GSC is used to eliminate the unbalanced voltage. Besides SVO control algorithms, a direct torque control (DTC) is proposed for induction machines [13,16]. DTC is a robust algorithm against changes in the machine parameters. A direct power control (DPC) algorithm is used in [17–20] to control DFIGs in wind power generation systems. In [17–20], the switching pattern of the DPC algorithm is directly selected from an optimal switching table according to the estimated rotor and stator data. Due to the hysteresis blocks used in DPC, the switching frequency is variable and the electromagnetic torque contains significant ripple. In addition, the output power includes some oscillations. To provide a fixed switching frequency in DPC, a direct power controlled space vector modulated (DPC-SVM) with complex design procedure is proposed in [21,22]. However, there are still some fluctuations in the electromagnetic torque and active and reactive powers. A sliding-mode controller (SMC) was recently introduced to control DFIGs connected to the ideal grid voltage [23–26]. Simple implementation and good robustness are the main merits of the proposed SMC. A grid with an unbalanced voltage is considered in [27], where the rotor current is decomposed to positive and negative sequences. Therefore, in [27], there is some error in the values of the tracked signals phase and amplitude. SMC is also used to design controllers of the rotor-side converter (RSC) and the grid-side converter (GSC) to control the electromagnetic torque and the system output power by under unbalanced and harmonic grid voltages in [28]. The technique used in [28] does not need to separate the positive and negative sequences of voltage or current. However, because of the PI controller in [28], some ripples in the DC-link voltage and the injected power to the grid are included, which decrease the output power quality. The presented paper removes the fluctuations and distortions in the DC-link voltage and the injected power to the grid.

The method presented in this paper is based on the SMC and controls the DC-link voltage, which overcomes the aforementioned problems. Simulation results show the effectiveness and superiority of the presented method for both transient and steady states. In addition, robustness with respect to parameter variations is the other advantage of the proposed algorithm. In section 2, modeling of DFIG, RSC, and GSC is discussed. The SMC for the both RSC and GSC are presented in section 3. In section 4, simulation results using MATLAB/Simulink software are presented. Finally, in Section 5, a discussion and conclusions of the work are provided to highlight the advantages of the proposed method.

2. System modeling

Figure 1 shows the considered grid-connected DFIG system, which is composed of RSC and GSC connected together through a DC-link. In the following, the models used of DFIG, GSC and RSC are presented.

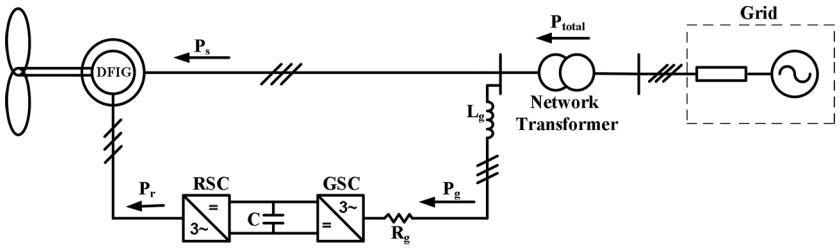

Figure 1. Configuration of the considered DFIG system.

2.1. DFIG modeling

The DFIG equivalent circuit in the stationary reference frame is shown in Figure 2, where $R_{s/r}$ and $L_{\sigma s/\sigma r}$ are the stator/rotor resistance and leakage inductances and L_m stands for the magnetizing inductance. The stator and rotor voltage components in the stator reference frame are as (1),

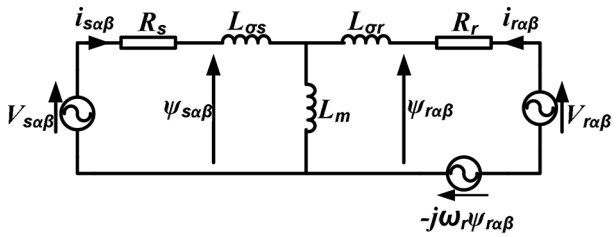

Figure 2. Equivalent circuit of DFIG.

$$\begin{aligned} V_{s\alpha\beta} &= R_s i_{s\alpha\beta} + \tfrac{d\psi_{s\alpha\beta}}{dt} \\ V_{r\alpha\beta} &= R_r i_{r\alpha\beta} + \tfrac{d\psi_{r\alpha\beta}}{dt} - j\omega_r \psi_{r\alpha\beta} \end{aligned} \tag{1}$$

where $i_{s\alpha\beta/r\alpha\beta}$ is the stator and rotor current and the stator/rotor flux linkages are expressed in (2).

$$\begin{aligned} \psi_{s\alpha\beta} &= L_s i_{s\alpha\beta} + L_m i_{r\alpha\beta} \\ \psi_{r\alpha\beta} &= L_r i_{r\alpha\beta} + L_m i_{s\alpha\beta} \end{aligned}, \tag{2}$$

The electromagnetic torque (T_e) and the stator reactive power are selected as the desired control variables, and they are obtained as (1).

$$\begin{aligned} T_e &= \tfrac{3PL_m}{2L_s}(i_{r\alpha}\psi_{s\beta} - i_{r\beta}\psi_{s\alpha}) \\ Q_s &= \tfrac{3}{2L_s}(\psi_{s\alpha}v_{s\beta} - \psi_{s\beta}v_{s\alpha}) + \tfrac{3L_m}{2L_s}(v_{s\alpha}i_{r\beta} - v_{s\beta}i_{r\alpha}) \end{aligned} \tag{3}$$

2.2. Modeling of GSC

The structure of the GSC used is shown in Figure 3. The voltage equation of the GSC in the stationary reference frame is as (4)

$$e_{\alpha\beta n} = U_{g\alpha\beta n} + R_g i_{g\alpha\beta} + L_g \frac{di_{g\alpha\beta}}{dt}, \tag{4}$$

where $e_{\alpha\beta n}$ is the grid side voltage in the stationary frame; $U_{g\alpha\beta n}$ is the voltage between the middle point of the convertor DC-link and the grid phase terminals and expressed as functions of U_{gaN}, U_{gbN}, and U_{gcN} in (5).

$$\begin{aligned} U_{g\alpha\beta n} &= \begin{bmatrix} U_{g\alpha n} \\ U_{g\beta n} \end{bmatrix} = M_2 M_1 \begin{bmatrix} U_{gaN} \\ U_{gbN} \\ U_{gcN} \end{bmatrix} \\ M_1 &= \tfrac{1}{3}\begin{bmatrix} 2 & -1 & -1 \\ -1 & 2 & -1 \\ -1 & -1 & 2 \end{bmatrix}, M_2 = \tfrac{2}{3}\begin{bmatrix} 1 & -0.5 & -0.5 \\ 0 & \frac{\sqrt{3}}{2} & -\frac{\sqrt{3}}{2} \end{bmatrix} \end{aligned}, \tag{5}$$

where M_1 is the 3-phase/2-phase transformation matrix and M_2 is the Clarke transformation matrix.

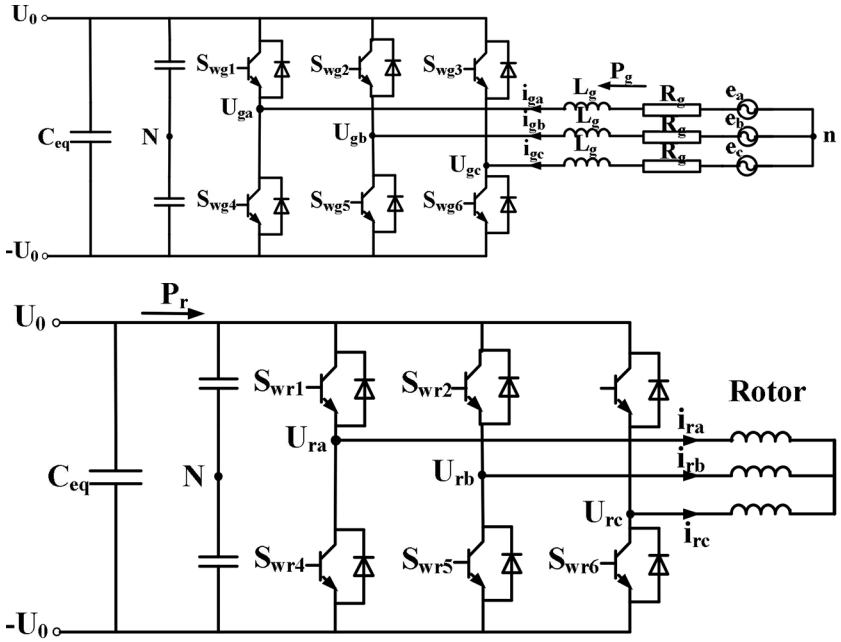

Figure 3. Structure of the used GSC (a) and RSC (b).

The state equation of the DC-link capacitor is as (6).

$$C_{eq}V_{dc}\frac{dV_{dc}}{dt} = P_g - P_e + P_s, \tag{6}$$

where P_e, P_g, and P_s are expressed in (7).

$$\begin{aligned} P_e &= \omega_r T_e \\ P_g &= \tfrac{3}{2}(e_{\alpha n} i_{g\alpha} + e_{\beta n} i_{g\beta}) \\ P_s &= \tfrac{3}{2}(V_{s\alpha} i_{s\alpha} + V_{s\beta} i_{s\beta}) \end{aligned} \tag{7}$$

According to Figure 1, the total active power and the GSC reactive power are defined in (8) and (9), respectively.

$$P_t = P_s + P_g \tag{8}$$

$$Q_g = \frac{3}{2}(e_{\beta n} i_{g\alpha} - e_{\alpha n} i_{g\beta}) \tag{9}$$

2.3. Modeling of RSC

The structure of the rotor side convertor is shown in Figure 3(b). U_{raN}, U_{rbN}, and U_{rcN} are voltages between the middle point of the convertor "N", and the rotor terminals and expressed as functions of the RSC switches state, S_{wr1}, S_{wr2}, ..., and S_{wr6}, in (10).

$$U_r = \begin{bmatrix} U_{raN} \\ U_{rbN} \\ U_{rcN} \end{bmatrix} = \frac{V_{dc}}{2} \begin{bmatrix} 1 & 0 & 0 & -1 & 0 & 0 \\ 0 & 1 & 0 & 0 & -1 & 0 \\ 0 & 0 & 1 & 0 & 0 & -1 \end{bmatrix} \begin{bmatrix} S_{wr1} \\ S_{wr2} \\ S_{wr3} \\ S_{wr4} \\ S_{wr5} \\ S_{wr6} \end{bmatrix} \tag{10}$$

The rotor voltage components in the stationary reference frame are obtained by (11).

$$\begin{bmatrix} U_{r\alpha} \\ U_{r\beta} \end{bmatrix} = M_3 M_2 M_1 \begin{bmatrix} U_{raN} \\ U_{rbN} \\ U_{rcN} \end{bmatrix}, \quad M_3 = \begin{bmatrix} \cos\theta_r & -\sin\theta_r \\ \sin\theta_r & \cos\theta_r \end{bmatrix} \tag{11}$$

where M_3 is the matrix that transfers the rotor reference frame into the stationary reference frame.

3. Proposed control strategy

3.1. RSC control algorithm

In Figure 4(a), the control scheme for the RSC is shown. The considered sliding surfaces are as (2) [28].

$$\begin{cases} S_{Te} = e_{Te} + c_{te} \int e_{Te} dt \\ S_{Qs} = e_{Qs} + c_{Qs} \int e_{Qs} dt \end{cases}, \tag{12}$$

where e_{Te} and e_{Qs} are error signals of the electromagnetic torque and the stator reactive power, respectively, and c_{Te} and c_{Qs} are the control gains.

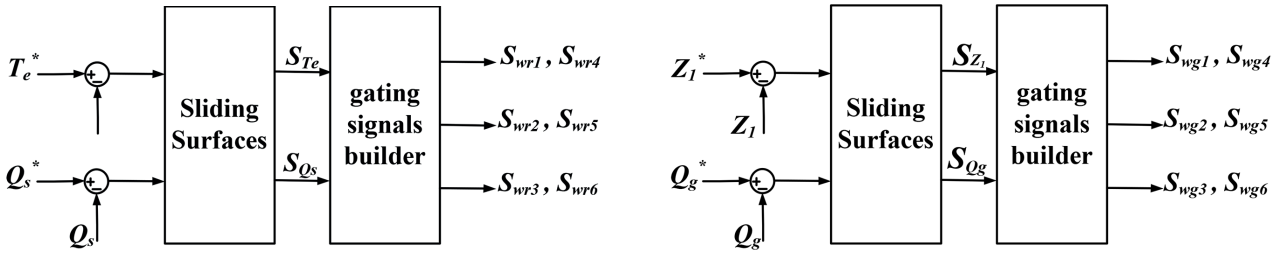

Figure 4. Proposed control scheme for RSC (a) and GSC (b) controllers.

3.2. GSC control algorithm

In this section, a new SMC scheme for GSC is designed. The structure of the used GSC is shown in Figure 4(b). As stated before, to have a robust controller against changes in the system parameters, especially against the DC-link voltage, SMCs are applied instead of the traditional PI controllers. Using SMCs the DC-link voltage is directly controlled and based on (6) and (7) the active power and the electromagnetic torque fluctuations are decreased. In addition, applying SMCs, the end line filters and compensator equipment could be removed, which results in a more economic design. These aspects are not found in the previous literature. The accuracy and effectiveness of the used controller for the GSC are confirmed by extensive dynamic simulations.

There is a direct relationship between the stator active power and the electromagnetic torque. At a constant DC-link voltage, if RSC eliminates electromagnetic torque fluctuations, based on (6) and (7), it is inferred that P_t remains free of fluctuations. According to (6), the first and second order derivations of DC-link

voltage are expressed as (13)

$$\begin{array}{l} \frac{dV_{dc}}{dt} = \frac{(P_g - P_e + P_s)}{C_{eq} V_{dc}}, \\ \frac{d^2 V_{dc}}{dt^2} = \frac{(\dot{P}_g - \dot{P}_e + \dot{P}_s)}{C_{eq} V_{dc}} - \frac{(P_g - P_e + P_s)^2}{C_{eq}^2 V_{dc}^3} \end{array} \tag{13}$$

Defining $Z_1 = \frac{1}{V_{dc}}$, the sliding surfaces yield as (14):

$$\begin{array}{l} S_{Z1} = \dot{e}_{Z1} + 2c_{Z1} e_{Z1} + c_{Z1}^2 \int e_{Z1} dt, \\ S_{Qg} = e_{Qg} + c_{Qg} \int e_{Qg} dt \end{array} , \tag{14}$$

where e_{Z1} and e_{Qg} are errors of Z_1 and reactive power, respectively, and presented in (15), and c_{Z1} and c_{Qg} are positive control gains.

$$\begin{array}{l} e_{Z1} = Z_1^* - Z_1, \\ e_{Qg} = Q_g^* - Q_g \end{array} \tag{15}$$

The dynamic performance of the switching variables is improved by deriving the sliding surfaces according to (16).

$$\begin{array}{l} \dot{S}_{Z1} = -\ddot{Z}_1 - 2c_{Z1} \dot{Z}_1 + c_{Z1}^2 \left(Z_1^* - Z_1 \right), \\ \dot{S}_{Qg} = \dot{Q}_g^* - \dot{Q}_g + c_{qg} (Q_g^* - Q_g) \end{array} \tag{16}$$

Using (13), and the derivation of (7), the variation in the active, reactive, and instantaneous electromagnetic powers can be calculated as (17).

$$\begin{array}{l} \dot{P}_g = \frac{3}{2} (\dot{e}_{\alpha n} i_{g\alpha} + e_{\alpha n} \dot{i}_{g\alpha} + \dot{e}_{\beta n} i_{g\beta} + e_{\beta n} \dot{i}_{g\beta}), \\ \dot{Q}_g = \frac{3}{2} (\dot{e}_{\beta n} i_{g\alpha} + e_{\beta n} \dot{i}_{g\alpha} - \dot{e}_{\alpha n} i_{g\beta} - e_{\alpha n} \dot{i}_{g\beta}), \\ \dot{P}_e = \dot{T}_e \omega_r + T_e \dot{\omega}_r \end{array} \tag{17}$$

Substituting (6), (13), and (17) into (16) yields (18).

$$\begin{bmatrix} \dot{S}_{Z1} \\ \dot{S}_{Qg} \end{bmatrix} = \begin{bmatrix} F_{Z1} \\ F_{Qg} \end{bmatrix} - B \begin{bmatrix} U_{g\alpha n} \\ U_{g\beta n} \end{bmatrix}, \tag{18}$$

where B is as (19), $e_{\alpha\beta n}$ are the components of the grid voltage in the stator reference frame, and g_1 and g_2 are functions of state variables as (20).

$$B = \frac{3}{2L_g} \begin{bmatrix} \frac{Z_1^3}{C_{eq}} e_{\alpha n} & \frac{Z_1^3}{C_{eq}} e_{\beta n} \\ -e_{\beta n} & e_{\alpha n} \end{bmatrix} \tag{19}$$

$$\begin{array}{l} F_{Z1} = g_1(\dot{e}_{\alpha n}, \dot{e}_{\beta n}, i_{g\alpha}, i_{g\beta}, \psi_{s\alpha}, \psi_{s\beta}, i_{r\alpha}, i_{r\beta}, \omega_r, i_{s\alpha}, i_{s\beta}, v_{s\alpha}, v_{s\beta}, e_{Z1}), \\ F_{Qg} = g_2(\dot{e}_{g\alpha}, \dot{e}_{g\beta}, i_{g\alpha}, i_{g\beta}, e_{Qg}, \dot{Q}_g^*) \end{array} \tag{20}$$

The sliding mode controller inputs are represented in (21) [29].

$$\begin{bmatrix} U_{gaN} \\ U_{gbN} \\ U_{gcN} \end{bmatrix} = \frac{V_{dc}}{2} sgn \begin{bmatrix} S_{ga} \\ S_{gb} \\ S_{gc} \end{bmatrix}, \tag{21}$$

where S_{gabc} will be defined later.

Replacing (5) and (21) into (18), (22) is obtained.

$$\begin{bmatrix} \dot{S}_{Z1} \\ \dot{S}_{Qg} \end{bmatrix} = \begin{bmatrix} F_{Z1} \\ F_{Qg} \end{bmatrix} - \frac{V_{dc}}{2} BM_2M_1 sgn \begin{bmatrix} S_{ga} \\ S_{gb} \\ S_{gc} \end{bmatrix} \tag{22}$$

It is suitable to select S_{gabc} as (23).

$$S_{gabc} = C^{+} \begin{bmatrix} S_{Z1} \\ S_{Qg} \end{bmatrix}, \tag{23}$$

where the C^{+} matrix is a pseudo-reverse one, which is expressed in (24).

$$\begin{aligned} &C^{+} = C^{T}\left(CC^{T}\right)^{-1} = \frac{2L_g}{3|e_{\alpha\beta n}|^2} \begin{bmatrix} \frac{C_{eq}}{Z_1^3} e_{\alpha n} & -e_{\beta n} \\ \frac{-C_{eq}}{Z_1^3}(e_{\alpha n} - \sqrt{3}e_{\beta n}) & \frac{1}{2}(e_{\beta n} + \sqrt{3}e_{\alpha n}) \\ \frac{-C_{eq}}{Z_1^3}(e_{\alpha n} + \sqrt{3}e_{\beta n}) & \frac{1}{2}(e_{\beta n} - \sqrt{3}e_{\alpha n}) \end{bmatrix} \\ &C = BM_2M_1 \end{aligned} \tag{24}$$

Replacing (23) and (24) into (21), the input controller signals are obtained. Finally, the control scheme for the GSC is shown in Figure 4, where S_{wg1}, S_{wg2}, ..., and S_{wg6} are the GSC switches state. Since the term $2L_g/(3je_n|^2)$ in C^{+} has no effect on the signs of S_{gabc}, the proposed GSC control algorithm is robust against parameter variations.

4. Simulation results

According to the developed model and the proposed control algorithm, some dynamic simulations have been carried out on the DFIG. The general block diagram for the proposed controller of the DFIG system is shown in Figure 5. To provide a thorough comparison of both previous and presented methods, the simulation parameters are adopted from [28]. These parameters are given in the Table. The performances of the both methods are compared with each other at different operating conditions to evaluate the effectiveness of the proposed controller. Simulations are carried out by MATLAB/Simulink. The simulations include the behavior of the DFIG in the network with unbalanced and harmonic voltages. In addition, the robustness of the proposed controller is investigated in the presented simulation results.

Table. Parameters of the simulated DFIG system.

Amount	Quantity	Symbol
2 MW	Nominal power	P_n
690 V/50 Hz	Rated r.m.s. stator voltage/frequency	V/f
2.6 mΩ	Stator resistance	R_s
77.306 mu H	Stator leakage inductance	$L_{\sigma s}$
2.5 mH	Magnetizing inductance	L_m
2.9 mΩ	Rotor resistance	R_r
83.369 mu H	Rotor leakage inductance	$L_{\sigma r}$
0.333	Stator/rotor turns ratio	n_1/n_2
2	Number of pole pairs	P
1200 V	DC-link rated voltage	V_{dc}
38 mF	DC-link equivalent capacitance	C_{eq}
0.25 mH	Grid-side line inductance	L_g
0.0 Ω	Grid-side line resistance	R_g

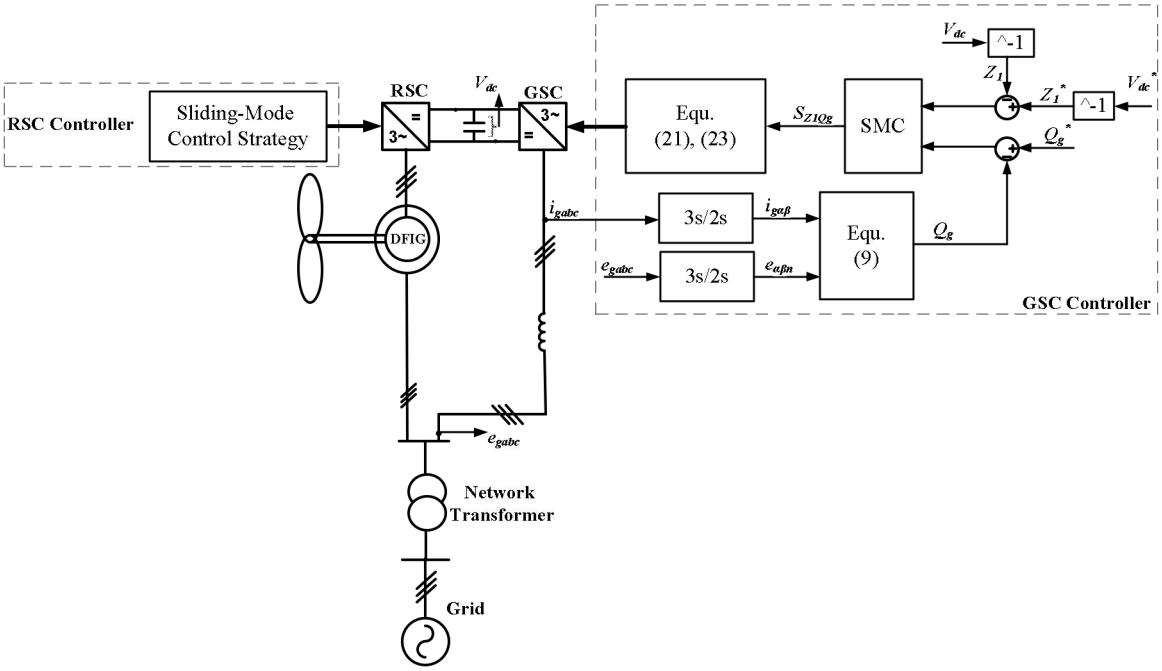

Figure 5. The control block diagram of the DFIG system.

4.1. Unbalanced voltage conditions

In the first simulation, the proposed controller is simulated and compared with the control method in [28] under unbalanced grid voltages with load variations. According to Figure 6(a), a 15% voltage drop is considered in two phases (A and C). The load changes at t = 5.5 (s) from T_e = 4 kN.m to T_e = 12 kN.m. In this simulation the rotor speed is 150 rpm. Figures 1(b)–1(d) show that, despite unbalanced voltage, the RSC controller is able to trace the reference values of the electromagnetic torque (Figure 6(b)) and stator active and reactive powers (Figure 6(c) and 6(d)). In addition, there are some fluctuations in the electromagnetic torque and stator reactive power in both control schemes. Therefore, SMC of the RSC for the proposed control method and the

control method in [28] has the same performance in the load variations. The other variables in the simulation are shown in Figure 7. To remove the fluctuations of the grid and the total active and reactive powers in [28], a proper control of the GSC is used in this paper. In the proposed method, by using the SMC in the GSC, the DC-link voltage and grid-side active and reactive powers do not have any fluctuation or distortion, as shown in Figure 7. This figure confirms that the proposed control method has a better performance in controlling system output power, and consequently it leads to more effective performance of the DFIG under voltage disturbance.

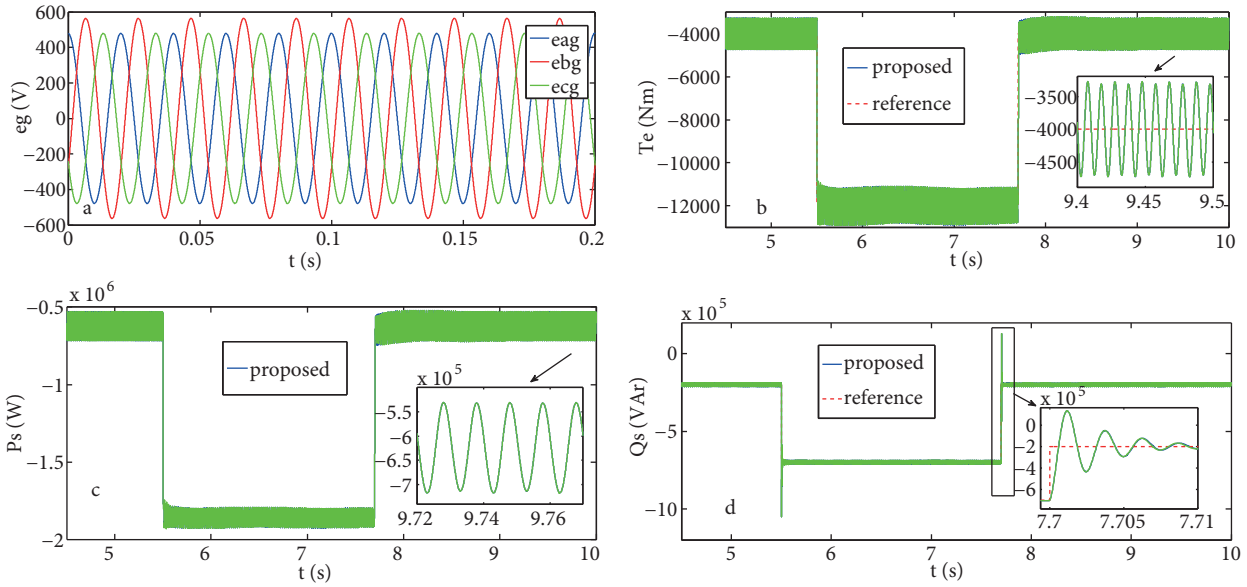

Figure 6. Simulation results under unbalanced voltage conditions: unbalanced three-phase voltage (a), electromagnetic torque (T_e) (b), active (P_s) (c), and reactive (Q_s) power (d).

4.2. Robustness test

In order to investigate the robustness of the system, it is supposed that the rotor and stator resistance (R_r, R_s) are increased up to 40% of their nominal values, while the magnetizing inductance (L_m), the grid-side line inductance (L_g), and the DC-link capacitance (C_{eq}) are decreased by the same rate. In addition, the unbalanced voltages are applied at the beginning of the simulation. Figure 8 shows that the method presented in [28] is not robust against parameter variation and become unstable in the mentioned parameter changing condition. The proposed control method is a robust procedure with very short transient time. The simulation results of the proposed control algorithm with and without the mentioned parameter variation are shown in Figure 9. The results with and without the parameter variations are marked by "B" and "A", respectively. The simulation results confirm that the proposed control method is robust against parameter variations. However, compared to the simulation results of the previous section, the amplitude of controlled variable oscillations is increased a little more.

4.3. Simulation results under harmonically distorted grid voltage conditions

In Figure 10, the simulation results of the proposed controller in a grid with unbalanced and harmonically distorted voltage are shown. The grid voltages include 6% of the fifth and 5% of the seventh order harmonics, which are dominant harmonics in the girds (Figure 10(a)). In this figure, despite harmonic distortions of voltage

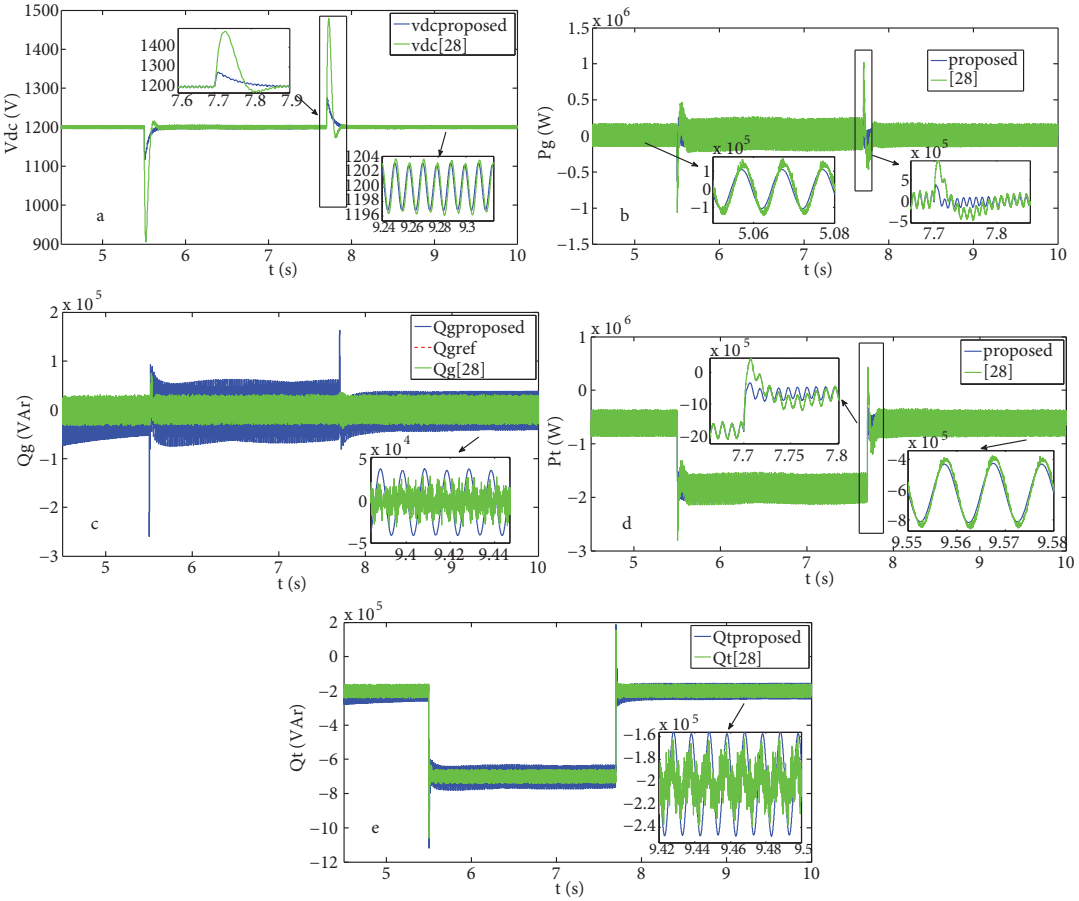

Figure 7. Simulation results under unbalanced voltage conditions: DC-link voltage (V_{dc}) (a), grid-side active power (P_g) (b), grid-side reactive power (Q_g) (c), total active power (P_t) (d), and total reactive power (Q_t) (e).

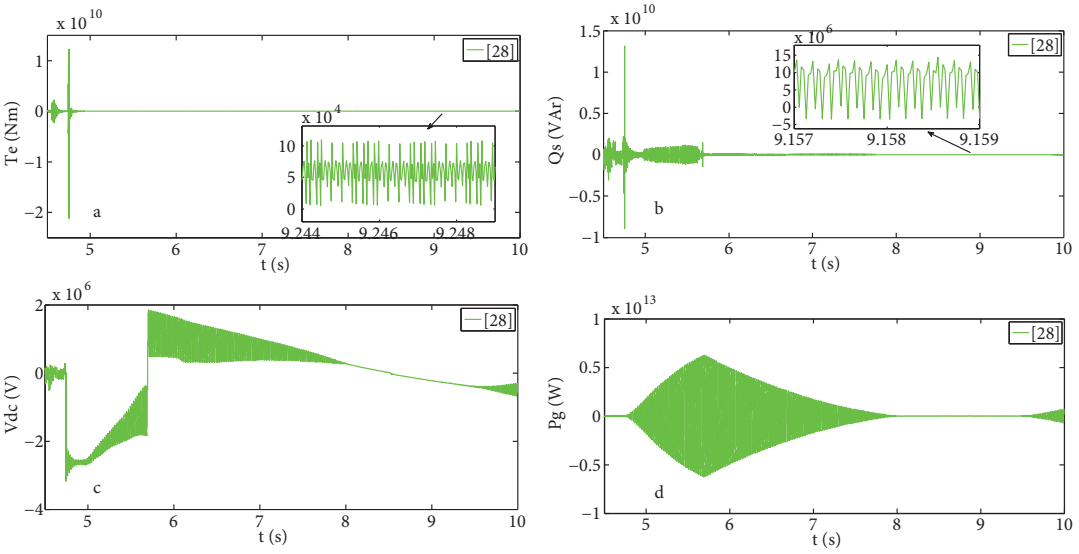

Figure 8. Simulation results of control methods of [28] against parameter variations: electromagnetic torque (T_e) (a), stator reactive power (Q_s) (b), DC-link voltage (V_{dc}) (c), grid-side active power (P_g) (d) under unbalanced grid voltages.

in both methods, the controllers are capable of controlling the electromagnetic torque and active and reactive powers (Figures 10(b)–10(f)). Moreover, in comparison with the method presented in [28], the ripple of DC-link voltage and the fluctuations of the injected active and reactive powers into the network are reduced considerably by using the suggested control method. All of the merits of the proposed control algorithm are because of the proper control for the GSC.

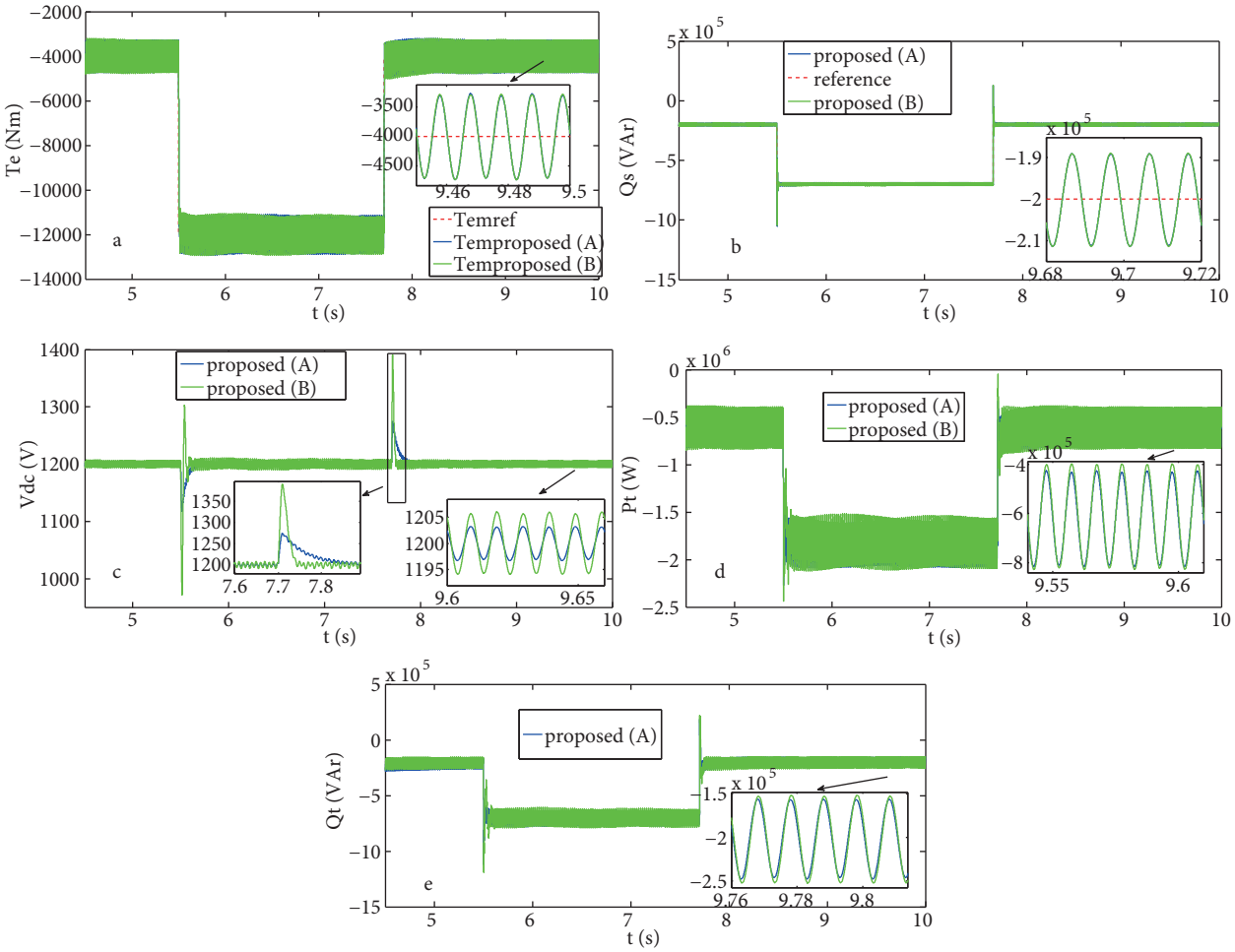

Figure 9. Simulation results of the proposed control method under unbalanced voltage conditions with (A) and without (B) parameter variations: electromagnetic torque (T_e) (a), stator reactive power (Q_s) (b), DC-link voltage (V_{dc}) (c), total active power (P_t) (d), and total reactive power (Q_t) (e).

5. Conclusions

In this paper a SMC-based algorithm is proposed for the DFIG. The novelty of the proposed controller over the previous algorithms is in the appropriate control of the GSC. It is shown that a desired performance is obtained for the DFIG under different conditions of unbalanced and harmonic distortion of grid voltage. A good performance is observed in transient and steady-state conditions. Since there is no need for extracting positive and negative sequences of voltage or current, the proposed method has a simple structure. In the proposed control method, the DC-link voltage is controlled by SMC. Therefore, there is a very small error in

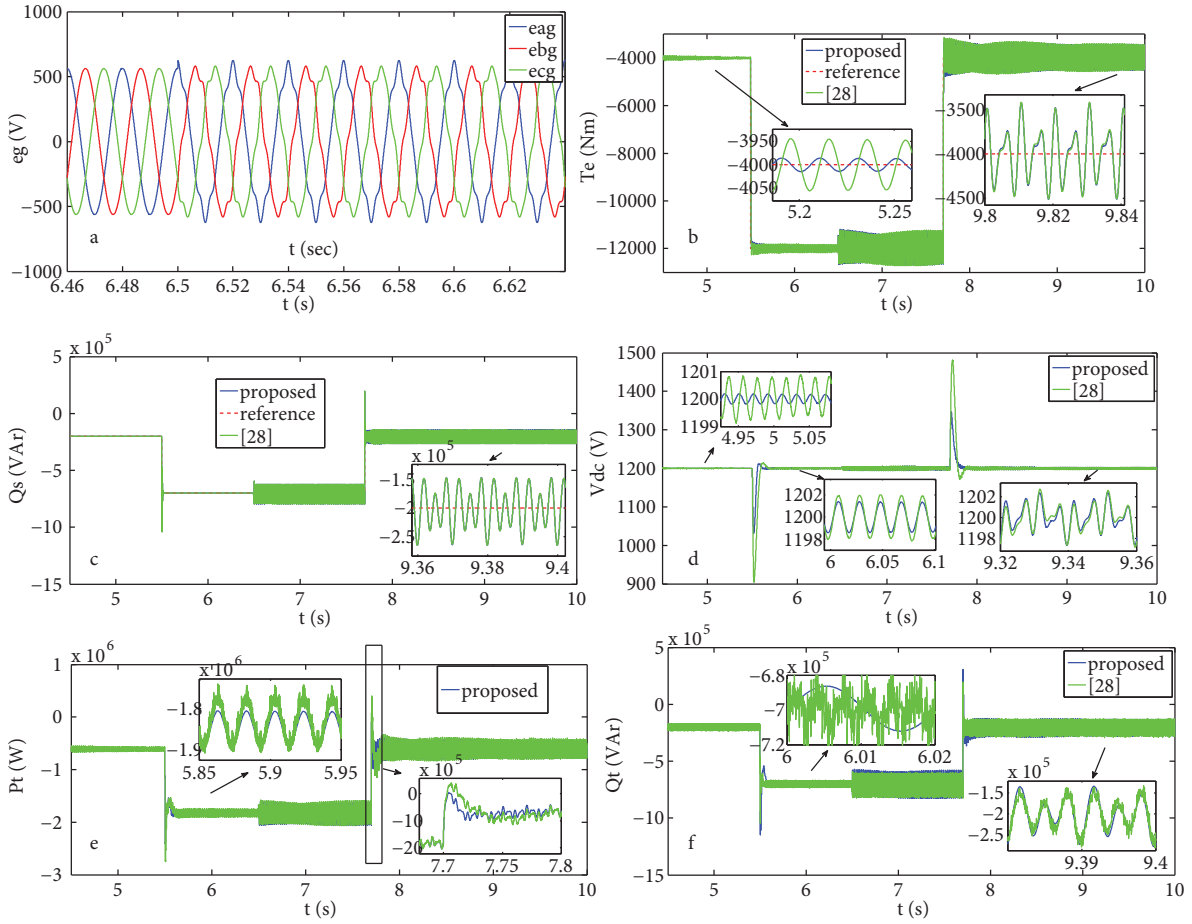

Figure 10. Simulation results under harmonically distorted grid voltage conditions: the grid voltages (a), electromagnetic torque (T_e) (b), the stator reactive power (Q_s) (c), DC-link voltage (V_{dc}) (d), total active power (P_t) (e), and the total reactive power (Q_t) (f).

the DC-link voltage with negligible voltage ripple. In addition, in comparison with PI control methods, the proposed control algorithm is more robust under system transient and steady-state conditions. Moreover, the difficulties of adjusting PI controller coefficients are eliminated. According to the simulation results, the system is also robust against parameter variations and has a fast dynamic response.

References

[1] Muljadi E, Batan T, Yildirim D, Butterfield C. Understanding the unbalanced-voltage problem in wind turbine generation. In: IEEE 1999 Industry Applications Conference; 3–7 October 1999; Phoenix; USA. New York, NY, USA: IEEE. pp. 1359-1365.

[2] Brekken T, Mohan N. A novel doubly fed induction wind generator control scheme for reactive power control and torque pulsation compensation under unbalanced grid voltage conditions. In: IEEE 2003 Power Electronics Specialist Conference; 15–19 June 2003; Acapulco; Mexico. New York, NY, USA: IEEE. pp. 760-764.

[3] Piwko R, Miller N, Sanchez J, Yuan X. Integrating large wind farms into weak power grids with long transmission lines. In: IEEE 2006 Power Electronics and Motion Control Conference; 14–16 August 2006; Shanghai; China. New York, NY, USA: IEEE. pp. 1-7.

[4] Kiani N, Lee W. Effects of voltage unbalance and system harmonics on the performance of doubly-fed induction wind generators. IEEE T Ind Appl 2010; 46: 562-568.

[5] Muller S, Deicke M, Doncker R. Doubly fed induction generator systems for wind turbines. IEEE T Ind Appl 2002; 8: 26-33.

[6] Hu J, He Y. Dynamic modeling and robust current control of wind-turbine used DFIG during AC voltage dip. J Zhejiang Univ Sci 2006; 7: 1757-1764.

[7] Pena R, Clare J, Asher GM. Doubly fed induction generator using back-to-back PWM converter and is application to variable-speed wind energy generation. Proc IEE Electr Power Appl 1996; 143: 231-241.

[8] Xu L, Cheng W. Torque and reactive power control of a doubly fed induction machine by position sensorless scheme. IEEE T Ind Appl 1995; 31: 636-642.

[9] Xu L, Wang Y. Dynamic modeling and control of DFIG based wind turbines under unbalanced network conditions. IEEE T Power Syst 2007; 22: 314-323.

[10] Xu L. Coordinated control of DFIGs rotor and grid side converters during network unbalance. IEEE T Power Electron 2008; 23: 1041-1049.

[11] Hu J, He Y. DFIG wind generation systems operating with limited converter rating considered under unbalanced network conditions-analysis and control design. Renewable Energy 2011; 36: 829-847.

[12] Hu J, He Y, Xu L, Williams B. Improved control of DFIG systems during network unbalance using PI-R current regulators. IEEE T Ind Electron 2009; 56: 439-451.

[13] Takahashi I, Noguchi T. A new quick-response and high-efficiency control strategy of an induction motor. IEEE T Ind Appl 1986; 22: 820-827.

[14] Petersson A. Analysis, modeling and control of doubly-fed induction generator for wind turbine. PhD, Chalmers University of Technology, Goteborg, Sweden, 2005.

[15] Yao J, Li H, Chen Z, Xia X, Chen X, Li Q, Liao Y. Enhanced control of a DFIG-based wind-power generation system with series grid-side converter under unbalanced grid voltage conditions. IEEE T Power Electron 2013; 28: 3167-3180.

[16] Depenbrock M. Direct self control (DSC) of inverter fed induction machine. IEEE T Power Electron 1988; 3: 420-429.

[17] Datta R, Ranganathan VT. Direct power control of grid-connected wound rotor induction machine without rotor position sensors. IEEE T Power Electron 2001; 16: 390-399.

[18] Xu L, Cartwright P. Direct active and reactive power control of DFIG for wind energy generation. IEEE T Energy Convers 2006; 21: 750-758.

[19] Abad G, Rodriguez MA, Poza J. Two-level VSC-based predictive torque control of the doubly fed induction machine with reduced torque and flux ripples at low constant switching frequency. IEEE T Power Electron 2008; 23: 1050-1061.

[20] Abad G, Rodriguez MA, Poza J. Two-level VSC-based predictive direct power control of the doubly fed induction machine with reduced power ripple at low constant switching frequency. IEEE T Energy Convers 2008; 23: 570-580.

[21] Kazemi MV, Yazdankhah AS, Kojabadi HM. Direct power control of DFIG based on discrete space vector modulation. Renewable Energy 2010; 35: 1033-1042.

[22] Zhi D, Xu L. Direct power control of DFIG with constant switching frequency and improved transient performance. IEEE T Energy Convers 2007; 22: 110-118.

[23] Hu J, Nian H, Hu B, He Y, Zhu Z. Direct active and reactive power regulation of DFIG using sliding-mode control approach. IEEE T Energy Convers 2010; 25: 1028-1039.

[24] Susperregui A, Tapia G, Zubia I, Ostolaza X. Sliding-mode control of doubly-fed generator for optimum power curve tracking. Electron Lett 2010; 46: 126-127.

[25] Machmoum M, Poitiers F. Sliding mode control of a variable speed wind energy conversion system with DFIG. In: International Conference on Ecological Vehicles and Renewable Energies; 26–29 March 2009; Monaco; France. New York, NY, USA: IEEE. pp. 1-7.

[26] Zheng X, Li L, Xu D, Platts J. Sliding-mode MPPT control of variable speed wind power system. In: IEEE 2009 Power and Energy Engineering Conference; 27–31 March 2009; Wuhan; China. New York, NY, USA: IEEE. pp. 1-4.

[27] Chen S, Cheung N, Wong K, Wu J. Integral sliding-mode direct torque control of doubly-fed induction generators under unbalanced grid voltage. IEEE T Energy Convers 2010; 25: 356-368.

[28] Itsaso M, Tapia G, Susperregui A, Camblong H. Sliding-mode control for DFIG rotor- and grid-side converters under unbalanced and harmonically distorted grid voltage. IEEE T Energy Convers 2012; 27: 328-338.

[29] Utkin V. Sliding-mode control design principles and applications to electric drives. IEEE T Ind Electron 1993; 40: 23-36.

A. Appendix

Nomenclature

v_s, e_n	Stator and grid voltage vectors
i_s, i_r	Stator and rotor current vectors
i_g	Grid-side converter current vectors
L_g	Grid-side line inductance
L_m, L_r, L_s	Magnetizing, rotor, and stator inductances
$L_{\sigma s}$, $L_{\sigma r}$	Rotor and stator leakage inductances
P	Number of pole pairs
P_e	Electromagnetic power
P_s, Q_s	Stator output active and reactive powers
P_r, Q_r	Rotor output active and reactive powers
P_g, Q_g	Grid-side converter output active and reactive powers
P_t, Q_t	Active and reactive powers from the overall system
C_{eq}	DC-link equivalent capacitance
R_g	Grid-side line resistance
R_r, R_s	Rotor and stator resistances
V_{dc}	DC-link voltage
θ_r	Rotor electrical position
ω_r	Rotor electrical speed

Subscripts

$\alpha\beta$	Stationary $\alpha\beta$-axis
s, r	Stator and rotor
g	Grid

Superscripts

$*$	Reference value

B. Appendix Control parameters.

Proportional and Integral gains, $K_P = 2800$ and $K_I = 100{,}920$
Positive gains, $c_{te} = 1$ and $c_{qs} = 1$
Positive gains, $c_{Z1} = 120$ and $c_{qg} = 1$